Effect of the formation of NiCu alloy and use of biomass-derived furfural on the catalytic hydrogenation of furfural to THFA

Vladimir Sánchez, Pilar Salagre, María Dolores González, Jordi Llorca, Yolanda Cesteros

[a] Department de Química Física i Inorgànica, Universitat Rovira i Virgili, 43007 Tarragona, Spain

[b] Institute of Energy Technologies and Centre for Research in Nanoengineering, Universitat Politècnica de Catalunya, Avda. Diagonal 647, ed. ETSEIB, 08028 Barcelona, Spain

Abstract

Several Ni, Cu and Ni-Cu catalysts supported on mesoporous hectorite were prepared, characterized and tested for the hydrogenation of commercial furfural to obtain tetrahydrofurfuryl alcohol (THFA). The highest selectivity to THFA (95 %) for a total conversion was achieved with the Ni-Cu catalyst prepared with a Ni:Cu molar ratio of 1:1 after 4 h of reaction. This can be explained by the formation of NiCu alloy in high amounts for this sample (88 %), as detected by XRD. The lower selectivity to THFA obtained with other bimetallic catalysts prepared with Ni:Cu molar ratios of 6:1 and 1:6 were attributed to the lower percentage of NiCu alloy together with the lowest Ni richness of the NiCu alloy. Additionally, the best catalyst resulted in a yield to THFA of 90 %, in the toluene phase, and 80 % in the aqueous neutralized phase, when using a biomass extract of furfural obtained from almond shells instead of commercial furfural. After several reuses of the catalyst employed in the toluene phase, some decrease of THFA was observed due to the increase of the crystallite size of the Cu phase, as observed by XRD, that should decorate the active NiCu alloy particles.

Introduction

The production of fuels and chemicals from biomass is becoming significant as an environmental alternative to their obtention from crude oil. Lignocellulose, the most abundant renewable biomass, is considered the main raw material on a biorefinery concept, since its non-edible nature does not compete with food crops and is less expensive than conventional agricultural feedstocks. Lignocellulose biomass consists of three types of polymers, cellulose (40–50 %), hemicellulose (25–35 %), and lignin (15–20 %). One of the challenges of biomass conversion is to obtain target molecules that can be later transformed into high-added value products. Furfural (FUR) is an important building block for the production of biobased chemicals. It is obtained by the catalysed dehydration of sugars from xylose, extracted from hemicellulose, which comes from agricultural waste materials, like corn cobs, oat shells, almond shells and hazelnut peels [1]. Furfural can be converted, through catalytic hydrogenation, into different products of interest, such as furfuryl alcohol (FOL), cyclopentanone (CPO) or tetrahydrofurfuryl alcohol (THFA) [2] THFA, which is the main hydrogenated product, can be used as an environmentally benign solvent. The traditional production of tetrahydrofurfuryl alcohol is carried out in two steps from furfural with furfuryl alcohol as intermediate (Scheme 1). The reaction can be performed in liquid or gas phase [3].

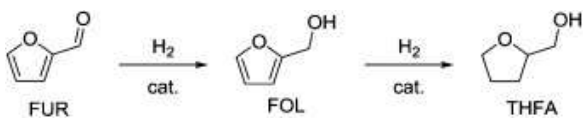

Scheme 1. Catalytic hydrogenation of furfural for the obtention of THFA.

The direct hydrogenation of furfural to THFA has been studied with noble metals and their alloys, with very good results especially for Pd, Rh and Ru [[4], [5], [6]]. Although the activity of these catalysts was good, their high cost and the fact that these elements are in high risk make necessary to look for catalysts based in non-noble metals. Among these, Ni [6] or Cu [7] has been considered. Good results were obtained with a monometallic nickel catalyst supported on carbon nanotubes at 403 K and 40 bars of H2 pressure after 10 h of reaction (84,3 % yield of THFA) [8], a Ni/C catalyst derived from MOFs at 393 K and 10 bars of H2 pressure after 2 h of reaction (total conversion and total selectivity to THFA) [9], and a Ni/γ-Al2O3 catalyst at 353 K and 40 bars of H2 pressure after 2 h of reaction (conversion up to 99,8 % and selectivity to THA of 99,5 %) [10]. However, problems of leaching difficult their reuse [2]. Nakagawa et al. developed a nickel supported on silica catalyst that achieved values of selectivity to THFA of 100 % and 94 % of yield at 403 K in the gas phase [11]. The authors propose that the mechanism of reaction involves a strong adsorption of furfural through CO bond (η2-C, O), which is attacked by two hydrogen atoms previously adsorbed, so that ends up achieving the FOL. To obtain THFA, the -CH2OH group from furfuryl alcohol is adsorbed on nickel surface. The rate-determining step is the hydrogenation of the furan, which evolves to the obtention of THFA. The use of bimetallic catalytic systems can favour the formation of interesting stable catalysts based in non-noble metals. Between these, Cu-Ni nanocatalysts has been shown to be very efficient in several reactions [8,12]. However, it is difficult to obtain an homogeneous composition, especially at high metal charge, since the standard reduction potential for Cu and Ni are very different. A good dispersion was obtained by using layered double hydroxides (LDH) of Ni and Cu as catalysts precursors [13]. A yield of 93 % towards THFA was obtained at 423 K, 40 bar of H2 pressure in 3 h, using ethanol as solvent. The most important byproducts, which are competing with the formation of THFA, are cyclopentanone (CPO), cyclopentanol (CPL) and humines. Humines are formed in acidic aqueous conditions, and can affect the catalytic activity since they can cover the catalyst surface.

More recently, bimetallic nickel-cobalt catalysts supported on SBA-15 achieved total conversion and 90,4 % of selectivity to THFA at 363 K, 70 bars of H2 pressure and 6 h of reaction [14] while bimetallic MOF derived Ni-Co alloy catalyst presented almost total conversion and 99,1 % THFA selectivity at 353 K, 30 bars of H2 pressure and 8 h of reaction [15]. In addition, several authors studied catalytic systems under very low temperatures. Ruan et al. reported high selectivity (90,0% and 92,4%) to furfuryl alcohol (FOL) at 278 K or 283 K respectively, 50 bars of H2 pressure and 1 h of reaction using a Pd/Ni/Ni(OH)2/C catalyst [16]. Nakagawa et al. reported the hydrogenation of furfural to THFA with high selectivity (94 %) in aqueous media using a Pd–Ir/SiO2 bimetallic catalyst at low temperature (275 K) after 6 h of reaction. However, high hydrogen pressure (80 bars) was required [17].

Hectorites (Mn+x/n·yH2O[Mg6-xLix](Si8)O20(OH.F)4), and related hectorite compounds, are layered materials with high cation exchange capacity (C.E.C.), and interesting surface and acidic properties [18], which make them suitable to be used as catalytic supports for this reaction. Indeed, high selectivity to THFA (>98,7 %) was observed in the hydrogenation of FOL at low-temperature (313 K) and 20 bars of H2 after 1 h of reaction using Ru nanoparticles intercalated in hectorite [19]. Delaminated hectorites can be synthesized using quaternary ammonium salts during the hydrothermal treatment, as proposed by Iwasaki et al. [20], or by preparing polymer-hectorite clays [21]. The mesoporous of delaminated hectorites are obtained after removing the template by

calcination leading to high surface areas. The mesopores correspond to antiparticle space of disk-shaped crystallites aggregated by edge-to-face bonding.

The aim of this work is the design of stable catalysts active for the hydrogenation of commercial furfural to THFA with a low contribution of acid sites to avoid side reactions. Several Cu, Ni and Ni-Cu catalysts supported on mesoporous hectorite will be prepared and widely characterized by XRD and XPS techniques. Mesoporous hectorite was chosen because of its interesting properties, such as high surface area and mesoporosity together with low cost. The best catalyst will be tested using a biomass extract, obtained from almond shells, as furfural source. The reusability of this catalyst will be also checked.

Experimental

Commercial reagents and materials

All commercial reagents were of analytical grade. Nickel nitrate hexahydrate, copper (II) nitrate hexahydrate, sodium silicate, nitric acid, magnesium chloride hexahydrate, lithium fluoride, trimethyldodecylammonium chloride (TMDACl) and furfural were purchased in Sigma-Aldrich, furfuryl alcohol in Alfa Aesar and tetrahydrofurfuryl alcohol in Acros Organics. Commercial furfural was distilled under reduced pressure before using. Grounded almond shells were obtained from UNIO Cooperative in Reus (Tarragona).

Preparation of catalysts

One mesoporous delaminated hectorite (DH) was prepared following the method previously developed in our research group [22,23]. The use of trimethyldodecylammonium chloride as template during the hectorite synthesis favoured its delamination resulting in a material with high surface area (353 m2/g). 25 mL of an ethanolic solution containing the appropriate amounts of Ni(NO3)2 and Cu(NO3)2 to have 40 wt % of metal in the final catalysts were added to 1 g of mesoporous hectorite using different Ni:Cu molar ratios: 1:0, 0:1, 6:1, 1:1 and 1:6. Then, the solvent was rotary-evaporated. The resulting solid was dried at 353 K overnight and calcined at 723 K for 5 h (P-Ni-DH, P-Cu-DH, P-Ni6Cu-DH, P-NiCu-DH and P-NiCu6-DH, respectively). Finally, the catalytic precursors were reduced in a fluidized bed tubular reactor at 1,25 mL/s of H2 flow at 723 K for 6 h (catalysts Ni-DH, Cu-DH, Ni6Cu-DH, NiCu-DH and NiCu6-DH).

Preparation of furfural from biomass

50 mL of 1 wt % sulfuric acid were added to 15 g of grounded almond shells. This mixture was heated at 393 K in a teflon autoclave reactor using microwaves (Milestone Ethos Touch Control, 400 W) for 1 h under stirring. The mixture was filtered and the liquid phase was stored as extract. 25 mL of toluene were added to 25 mL of this extract and heated at 433 K in a teflon autoclave reactor using microwaves (400 W) for 4 h under stirring. Both organic and aqueous phases were separated and stored on the fridge. Furfural concentrations were determined by gas chromatography. The average concentrations of furfural were: 4 g/L in the aqueous phase and 16 g/L in the toluene phase.

Characterization techniques

X-Ray diffraction was used to identify and quantify the crystalline phases present in the catalytic precursors and catalysts. The experiments were carried out with a Siemens D5000 diffractometer (Bragg–Brentano parafocusing geometry and vertical θ–θ goniometer) fitted with a curved graphite diffracted-beam monochromator and diffracted-beam Soller slits, a 0.06° receiving slit, and scintillation counter as a detector. The angular 2θ diffraction range was between 5 and 70°. Sample was dusted on to a low background Si (510) sample holder. The data were collected with an angular step of 0.05° at 3 s per step and sample rotation. CuKα radiation was obtained from a copper X-ray tube operated at 40 kV and 30 mA. The JCPDS files used for the identification of the crystalline phases were 00-003-0168, 01-077-9326, 00-004-0836, 00-047-1049, 00-048-1548, 01-083-3568, for hectorite, Ni, Cu, NiO (bunsenite), CuO (tenorite), Cu2O, respectively. The relative quantitative phase analysis was obtained by refining the Rietveld scale factor for each phase, and applying the corresponding well-known equations [24]. The peak width of each phase was modelled with the Double-Voigt Approach [25] by considering only the Lorentzian contribution of the crystallite size effect and discarding any contribution of the microstrain to the peak width. The averaged integral breadth was obtained from the resulting fitted Voigt function to the whole diffractogram. Crystallite size of the catalysts was determined by Rietveld refinement [26] using the TOPAS v6 software [27,28]. The background was modelled with a 2nd order Chebyschev polynomial. The instrumental contribution to the diffraction profile was calculated with the Fundamental Parameters Approach [29]. The Scherrer equation [30] was then applied to obtain the apparent crystallite size.

The reducibility of the catalyst precursors was analyzed by using an Autochem AC2920 Micrometric apparatus equipped with a thermal conductivity detector (TCD). For each experiment, 100 mg of sample was heated between room temperature and 1173 K at a rate of 10 K/min under a flow of 5 % H2 in argon (50 mL/min). The amount of hydrogen consumed was monitored by TCD.

Environmental scanning electron microscopy (ESEM) combined with energy dispersive X-ray (EDX) microanalysis were performed to confirm the presence of NiCu alloy using a JEOL 6400 electron microscope (3.5 nm resolution at 20 kV) fitted with an energy-dispersive X-ray spectrometer (Inca-Energy, Oxford Instruments) and Si(Li) detector with 1.38 eV energy resolution.

X-ray Photoelectron Spectroscopy (XPS), which was used for the surface characterization of the catalyst precursors, was performed with a SPECS system equipped with an Al anode XR50 source operated at 150 W and a Phoibos MCD-9 detector. The pressure in the analysis chamber was kept below 10−7 Pa. The area analyzed was approximately 2 mm x 2 mm. The pass energy of the hemispherical analyzer was set at 25 eV, and the energy step was fixed at 0.1 eV. Powdered samples were pressed to self-supported pellets. Data processing was carried out with the Casa XPS program (Casa Software Ltd., UK). The binding energy (BE) values were referenced to the C1s peak at BE = 284,8 eV.

Catalytic activity

Catalytic hydrogenation of furfural was performed in a 50 mL stainless steel autoclave equipped with a stirrer, a pressure valve and automatic temperature control apparatus. The reactor was connected to hydrogen flow. When using commercial furfural: 30 mL of 50 g/L aqueous solution of commercial furfural was added together with 600 mg of catalyst. For the catalytic tests with the furfural

obtained from biomass, 30 mL of the aqueous or organic phase was added with the same amount of catalyst. Then, the reactor was sealed and purged three times with H2 for air removal. Afterwards, H2 was fully charged into the reactor until 40 bar pressure, and heated up to 413 K and 600 rpm during the corresponding reaction time (0,5, 1, 2 or 4 h). Reaction products were analysed by gas chromatography (GC).

For reusability tests, catalyst was separated from the toluene solution of the furfural extract by centrifugation (5 min at 4000 rpm), then cleaned with ethanol by centrifugation for three times, and finally dried under a nitrogen flow. Before each reuse, catalyst was activated in a fluidized bed tubular reactor with 1,25 mL/s of H2 flow at 723 K for 2 h.

Analysis of the reaction products

GC measurements were performed on Shimadzu GC-2010A series equipped with AOC-20i Series autoinjector and FID. The column was a Suprawax-280 (60 m x 0,25 µm × 0,50 µm). 1-Butanol was the internal standard. The quantification of products was determined based on GC data using the internal standard method in order to determine the conversion and selectivity of the main products.

Results and discussion

Characterization of the catalytic precursors

Fig. 1 shows the XRD patterns of the catalytic precursors. Quantification of the metal oxide phases and their crystallite sizes are indicated in Table 1. No peaks due to the starting metal nitrates were detected in any case. All samples exhibited the characteristic low-crystalline peaks attributed to the hectorite phase (indicated with * on the figure). The absence, at lower angles (2θ = 0–10), of the peak corresponding to the 001 reflection, related to the layer stacking, confirmed the delamination of the hectorite. XRD patterns of the catalytic precursors P-Cu-DH and P-Ni-Cu-DH showed the presence of the peaks due to the monoclinic CuO phase, and cubic NiO phase, respectively. Regarding the XRD patterns of the Ni-Cu catalytic precursors, some differences arise. Thus, for the Ni-Cu sample with the highest Ni content (P-Ni6Cu-DH), only the peaks corresponding to the NiO phase were detected. This could be explained by the lower detection limit of the XRD equipment for the CuO, which is present in low amounts in this sample. In our opinion, the other possible explanation, which could be a lower crystallinity of the CuO can be discarded taking into account the higher crystallite size of the CuO, when detected for the other NiCu samples, compared to the crystallite size of NiO, as commented below. For P-NiCu-DH, prepared with a Ni:Cu molar ratio 1:1, the peaks corresponding to NiO and CuO phases were clearly identified. Additionally, a new phase corresponding to Cu2O was observed for this sample (11 %, Table 1). This could be related to the oxidation of some Ni(II) atoms to Ni(III), allowing then the reduction of some Cu (II) atoms to Cu (I), increasing the well-known non-stoichiometry of nickel oxide. Finally, XRD pattern of P-NiCu6-DH showed mainly the presence of the CuO phase together with NiO and Cu2O in lower amounts (Table 1).

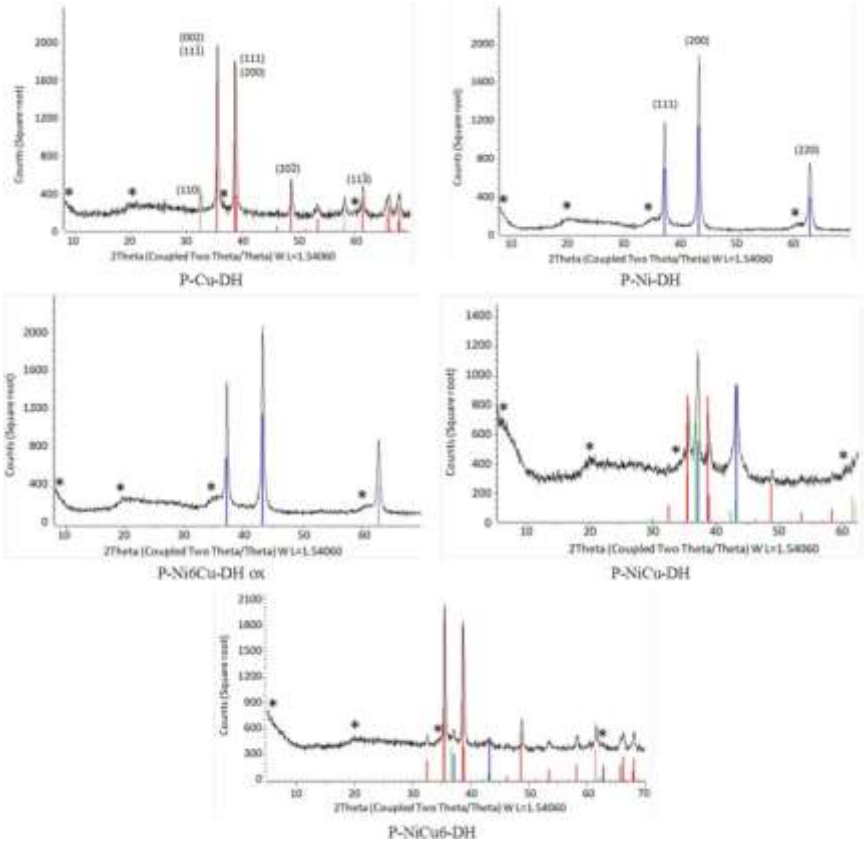

Fig. 1. XRD results of the catalytic precursors for all catalysts. * hectorite phase; red line: CuO phase; blue line: NiO phase; green line: Cu2O phase. (For interpretation of the references to colour in this figure legend, the reader is referred to the web version of this article).

Table 1. Characterization of the catalytic precursors by XRD.

Catalytic precursors	Crystalline phases (%)			Crystallite size (nm)[a]		
	CuO	NiO	Cu_2O	CuO	NiO	Cu_2O
P-Ni-DH	--	100	--	--	17,6	--
P-Ni6Cu-DH	--	100	--	--	17,7	--
P-NiCu-DH	20	69	11	33,0	5,8	44,0
P-NiCu6-DH	72	25	3	37,0	2,4	*
P-Cu-DH	100	--	--	39,7	--	--

[a] Calculated using Scherrer equation.

* It was not possible to calculate it.

The formation of solid solution between both metal oxides was not observed for any of the NiCu catalytic precursors. This can be explained by the different crystal structure of both oxides. From these results, we can conclude that there are independent particles of NiO, CuO and Cu2O in these catalytic precursors.

Regarding the crystallite sizes of the metal oxides summarized in Table 1, we can observe that crystallite sizes of CuO and Cu2O were noticeably higher than those of the NiO crystalline phase in all cases. An increase in the Cu content for the catalytic precursors resulted in an increase of the CuO crystallite size together with a decrease of the NiO crystallite size. It is well known that Cu(NO3)2 starts decomposing at lower temperatures than Ni(NO3)2 [31] so, when NiO crystals starts growing, there are crystals of CuO already formed that block the NiO growth. Additionally, nickel nitrate is less soluble in ethanol than copper nitrate. As a consequence, nickel nitrate deposited first, leading to less sites for copper nitrate to deposit resulting in less dispersed copper particles with higher crystallite sizes. Interestingly, for sample P-Ni6Cu-DH, CuO did not affect the crystallization of NiO, which had a similar crystallite size than the NiO of the sample P-Ni-DH, which does not contain copper. This can be explained because of the much lower amount of CuO in this sample. In order to confirm the presence of Ni (III) species on the catalytic precursors in which Cu2O was detected by XRD, XPS experiments were performed for P-NiCu-DH and Ni-DH for comparison (Fig. 2).

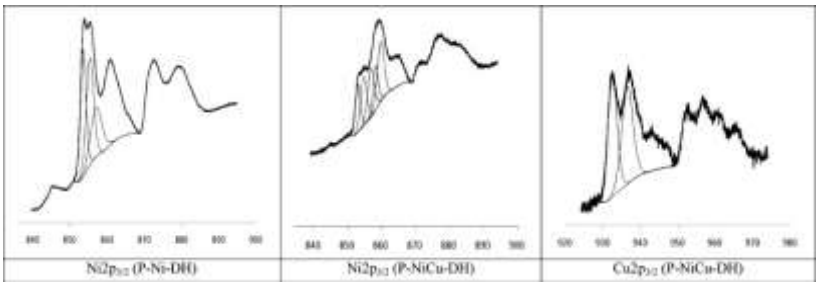

Fig. 2. XP spectra for Ni2p3/2 and Cu2p3/2 regions for P-Ni-DH and P-NiCu-DH containing catalytic precursors.

The Ni 2p3/2 regions of both samples were deconvoluted into two main overlapping signals with BEs at 853.1–854.8 and 857.0–858.9 eV. The lower BE component is ascribed to NiO, and the higher BE component is attributed to Ni (III) species, taking into account that higher oxidation states involves higher energy binding [32,33]. The presence of Ni (II) and Ni (III) species can be explained by the very well-known non-stoiochiometric character of NiO, which was confirmed by the black colour observed for this sample. Interestingly, the peak corresponding to Ni (III) increased for the NiCu oxide samples (Fig. 2). The Cu2p3/2 XP spectra of the P-NiCu-DH also confirmed the presence of two main overlapping peaks at 932.9 and 936.8 eV by deconvolution of the Cu 2p3/2 signal. The peak at 932.9 eV can be attributed to the reduced Cu species, probably the Cu2O detected by XRD, while that at higher binding energy of 936.8 eV can be assigned to CuO [32,33]. The reducibility of the hectorite supported metal oxides was studied by temperature-programmed reduction (Fig. 3).

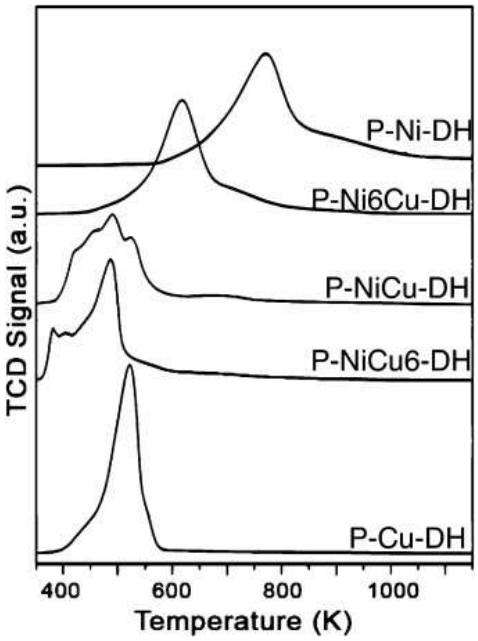

Fig. 3. TPR profiles for the catalytic precursors.

The reducibility of metal oxides to their corresponding metals depends on many factors, such as the nature and particle size of the metals together with its interaction with the support [34]. For monometallic samples (P-Cu-DH and P-Ni-DH), one main reduction peak was observed accompanied by several shoulders around it. The reducibility of CuO was considerably higher than that observed for NiO. This will be later confirmed by the XRD results of the catalysts. The profile of P-Ni6Cu-DH (the bimetallic sample with the highest Ni content) was similar to that of P-Ni-DH but a clear shift of the main reduction peak to lower temperatures was observed. This means that the presence of CuO, even in low amounts, favoured the reducibility of the NiO present in this sample. By increasing the Cu content (P-NiCu-DH and P-NiCu6-DH), we observed the appearance of new reduction peaks that can be related to the interaction between Ni species but especially the different Cu species (CuO and Cu2O) with the support, increasing the reducibility of both samples.

Characterization of catalysts

XRD of the catalyst Cu-DH showed the presence of the peaks corresponding to the Cu crystalline phase while the XRD of catalyst Ni-DH exhibited peaks, which can be assigned to NiO and Ni phases (Fig. 4). This agrees with the reducibility studies previously performed for their corresponding catalytic precursors by TPR.

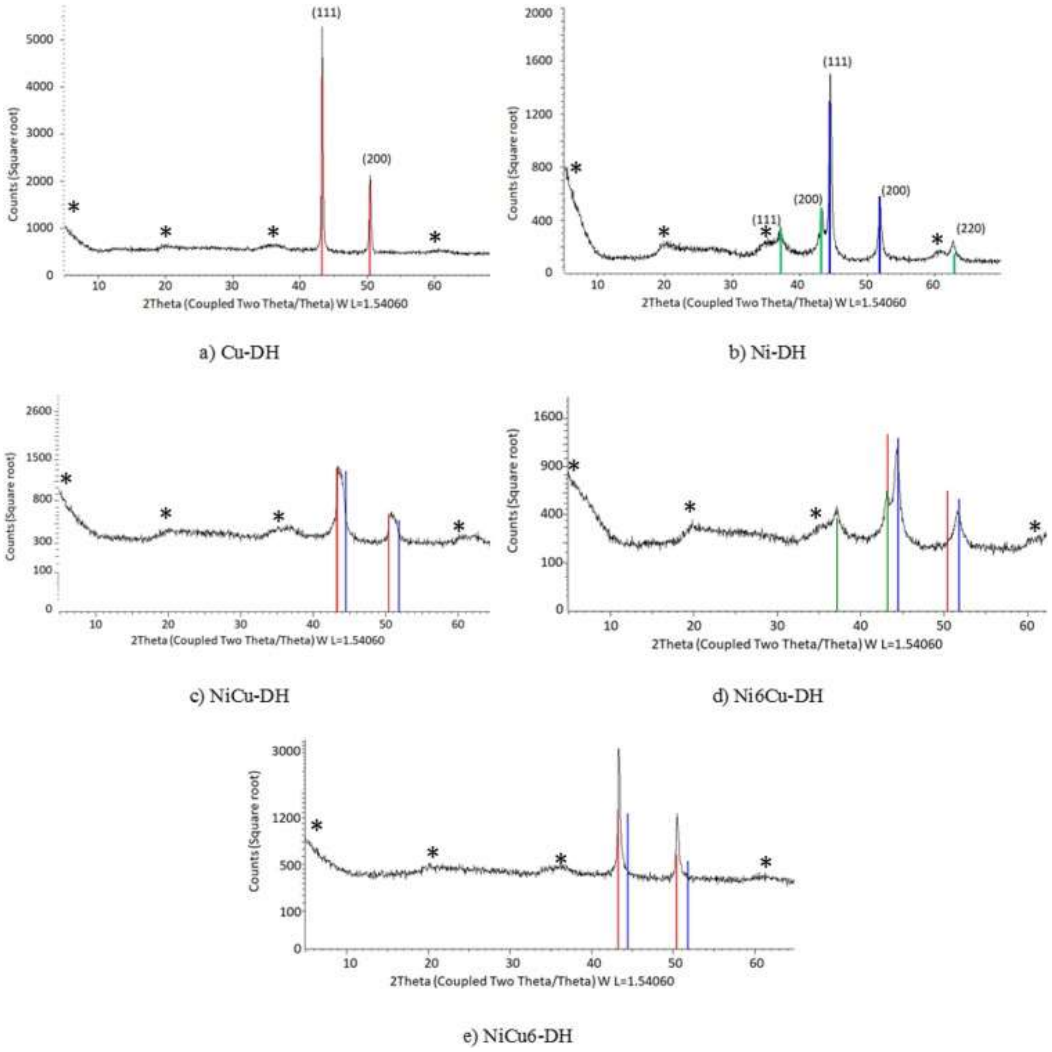

Fig. 4. XRD patterns of the catalysts. * hectorite phase; red line: Cu phase; blue line: Ni phase and green line: NiO phase. (For interpretation of the references to colour in this figure legend, the reader is referred to the web version of this article).

Interestingly, for bimetallic catalysts, we observed the formation of a Ni-Cu alloy for all samples since the peaks of the metallic phase shifted with respect to the corresponding positions of pure metallic Cu and Ni (Fig. 4). Thus, by comparing the XRD pattern of the catalysts Cu-DH, CuNi-DH and Ni-DH in the range 2Θ (40−50º) (Fig. 5), the position of the peak corresponding to the 111 reflection for the CuNi-DH catalyst was clearly located at 2θ = 43.5° between the position of metallic Cu (2θ = 44.0°) for Cu-DH and metallic Ni (2θ = 45.0°) for Ni-DH. The fact that all NiO was reduced for this bimetallic catalyst confirmed a positive interaction between Cu and Ni in terms of reducibility. It is important to have in mind that Ni and Cu crystallizes in the same crystalline structure, the face-centred cubic unit cell. Despite the oxides did not form a solid solution, once reduced, both metals rearrange into the same crystalline phase forming an alloy.

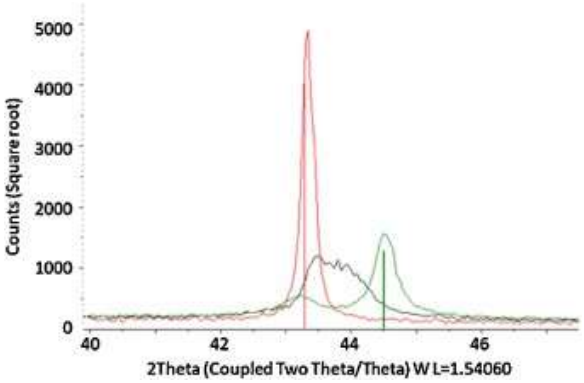

Fig. 5. Position of the peak corresponding to reflection 111 for Cu-DH (red line), NiCu-DH (black line) and Ni-DH (green line). (For interpretation of the references to colour in this figure legend, the reader is referred to the web version of this article).

XRD pattern of the catalyst with the highest Ni content (Ni6Cu-DH) showed the presence of NiO in addition to the Ni-Cu alloy phase (Fig. 4). This means that all the reduced Ni is forming alloy with Cu, and confirms the lower reducibility of NiO with respect to the copper oxides. In contrast, for the catalyst with the highest Cu content (NiCu6-DH), it was more difficult to distinguish between the NiCu alloy and the crystalline Cu formed since the signals were very close but nor NiO nor Ni was detected (Fig. 4). Therefore, from these results, we can conclude that all metallic Ni is taking part of the alloy for these catalysts, but in different amounts depending on the Ni:Cu ratio.

Fig. 6 shows the adjustment performed from the XRD patterns of bimetallic catalysts by using the Rietveld method in order to quantify their crystalline phases. The quantification results together with the calculation of the crystallite sizes are indicated in Table 2 for all catalysts.

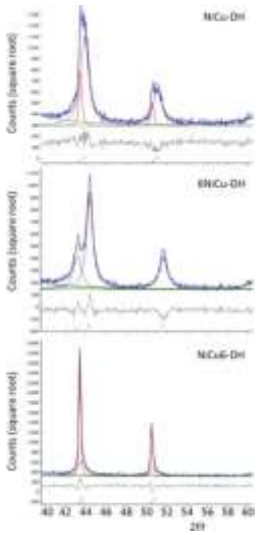

Fig. 6. Adjustment of the crystalline phases for bimetallic catalysts using the Rietveld method. Cu (red line); CuNi alloy (violet line); NiO (green line). (For interpretation of the references to colour in this figure legend, the reader is referred to the web version of this article).

Table 2. Characterization of the catalysts by XRD.

Catalysts	Crystalline phases (%)				Crystallite size (nm)[a]		
	Ni	Cu	NiO	NiCu Alloy	Ni	Cu	NiCu Alloy
Ni-DH	60	--	40	--	16,4	--	--
Ni6Cu-DH	--	--	40	60	--	--	9,0
NiCu-DH	--	12	--	88	--	31,8	6,6
NiCu6-DH	--	60	--	40	--	63,0	6,6
Cu-DH	--	100	--	-- --	58,3	--	

[a] Calculated using Scherrer equation.

It is important to remark that for bimetallic catalysts not only the percentage of alloy was different but also the percentage of Ni and Cu in the alloy were different regarding the Ni:Cu molar ratio and the phases present for each one. Both factors could affect the catalytic activity results. The NiCu ratio calculated from the cell parameter of the NiCu alloy phase according to the Vegard's law for these catalysts was NiCu1.14 for NiCu-DH, NiCu11 for NiCu6-DH and Ni5Cu for Ni6Cu-DH. These results also showed that all NiCu alloys were rich in copper. This is consistent with the results previously reported in the literature regarding bimetallic Ni-Cu systems [35,36], and has been justified on thermodynamics since the lower heat of sublimation of copper compared to nickel results in a higher occupation of surface sites of the bimetallic particles by copper [36]. The crystallite size was always higher for metallic copper particles being the alloy ones the smallest (Table 2). This involves higher particle dispersion when both metals come together, confirming again an interaction between metals.

Fig. 7 shows the scanning electron micrograph and the elemental Ni and Cu distribution map obtained by ESEM-EDX for catalyst NiCu-DH. The distribution of Ni and Cu was quite homogeneous along the sample. The proximity observed between red and green points, due to Ni and Cu, respectively, could confirm the formation of the NiCu alloy, in agreement with the results previously reported by other authors [37].

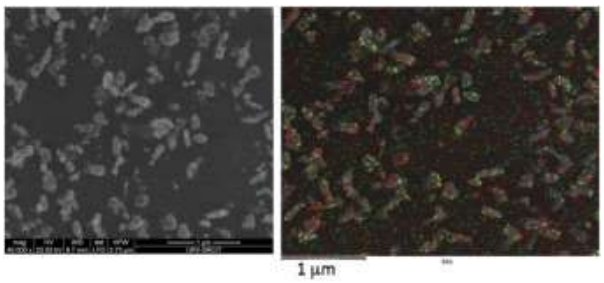

Fig. 7. ESEM image and Ni and Cu mapping obtained by EDX for catalyst NiCu-DH. Ni: red points; Cu: green points. (For interpretation of the references to colour in this figure legend, the reader is referred to the web version of this article).

Catalytic activity

Ni, Cu and NiCu catalysts were evaluated for the hydrogenation of commercial furfural to obtain THFA. First at all, we studied the effect of the reaction time, from 0.30 h to 4 h, on the yield to THFA using NiCu-DH catalyst (Fig. 8).

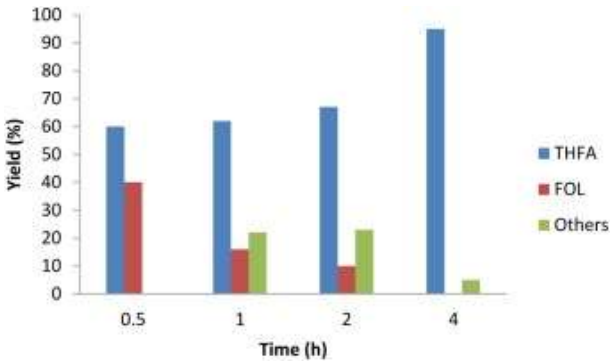

Fig. 8. Products yield values in function of the reaction time for NiCu-DH catalyst.

For all the reaction times, conversion was total. An increase in the reaction time clearly resulted in an increase of the yield to THFA, which was 95 % after 4 h or reaction. Furfuryl alcohol is an intermediate in the hydrogenation of furfural to THFA (Scheme 1). Then, the FOL yield decreased with time while THFA yield increased as far as FOL was transformed into THFA, as expected. No other reaction products were detected by gas chromatography. The other products until 100 % should be mainly polymerization products, such as humines, due to the acid catalysis. The amount of other products decreased by increasing the reaction time. This could be related to a higher hydrogenation capacity of the catalysts with time probably due to some deactivation of the acid centres. From these results, we established 4 h as the reaction time for the next experiments.

In order to study the influence of the formation of the NiCu alloy on the catalytic activity, monometallic and bimetallic catalysts, previously prepared, were tested for this reaction (Fig. 9). Delaminated hectorite, which was also checked to observe its influence, led to low conversion (33 %) and null selectivity to THFA, as expected, because of the absence of metallic phase, responsible for hydrogenation.

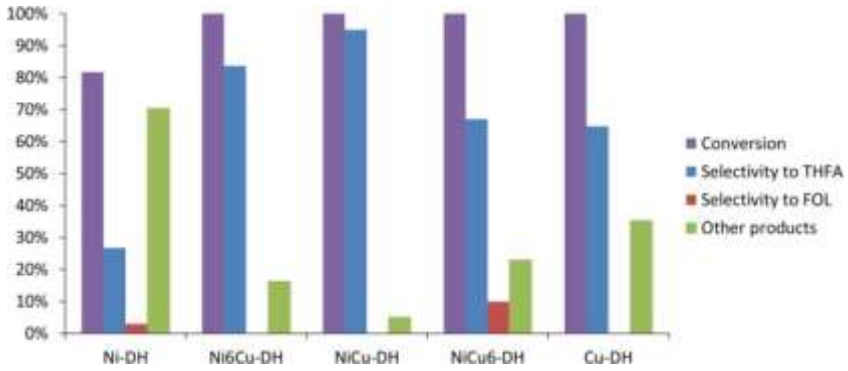

Fig. 9. Hydrogenation of furfural for all catalysts.

Regarding monometallic catalysts, Cu-DH showed higher conversion and higher selectivity to THFA than Ni-DH. This can be explained by the higher amount of metallic phase in Cu-DH since for Ni-DH, NiO was not totally reduced. Interestingly, by comparing the bimetallic catalysts, the catalyst which had the highest amount of NiCu alloy (Table 2), NiCu-DH, led to the highest selectivity to THFA (95 %) for a total conversion. Regarding Ni6Cu-DH and NiCu6-DH catalysts, the higher selectivity to THFA achieved by Ni6Cu-DH should be related to the highest amount of NiCu alloy present in this sample together with the expected higher amount of Ni present in the alloy, as deduced from its Ni:Cu molar ratio. Fig. 10 shows the representation of the % yield to THFA with respect to the % of NiCu alloy for bimetallic catalysts.

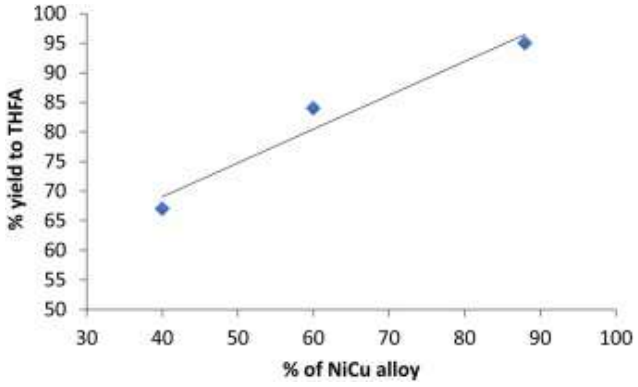

Fig. 10. Representation of % yield to THFA versus % of NiCu alloy content for NiCu catalysts.

As we can observe, there is a clear correlation between the yield to THFA and the percentage of the NiCu alloy present in the catalysts, confirming the activity of the alloy phase for this reaction. In order to check the activity of the best catalyst, NiCu-DH was tested using a biomass extract containing furfural instead of commercial furfural. As commented in the experimental section, furfural is obtained in two phases with concentrations values of 4 g/L in the aqueous phase and 16 g/L in the toluene phase. The reaction was performed for each phase separately. The aqueous phase is acid, due to the extraction procedure, and for this reason, two different tests were made for this phase, one directly and the other after previous neutralization. The catalytic results are shown in Table 3.

Table 3. Catalytic results when using furfural obtained from biomass.

Biomass extract phase		Yield (%)		
		THFA	FOL	Others
toluene		90	0	10
aqueous	neutralized	80	0	20
	acid	0	0	100

Total conversion was obtained for all phases. Regarding selectivity, FOL was not obtained in any case. For toluene and neutralized aqueous phases, this can be mainly attributed to its transformation to THFA (80–90 % yields) and additionally to the formation of other byproducts. Although these yields look similar, it is important to keep in mind that toluene solution of furfural was much more concentrated, four times, than the aqueous one. In the acid aqueous solution, neither THFA nor FOL were obtained. It is well known that furfural in acidic medium tends to polymerize into humines. Therefore, we can conclude that a non-acidic medium is crucial for this reaction in order to make effective the metallic sites for hydrogenation. Finally, catalyst NiCu-DH was reused 3 times at the conditions commented in the experimental section (Fig. 11).

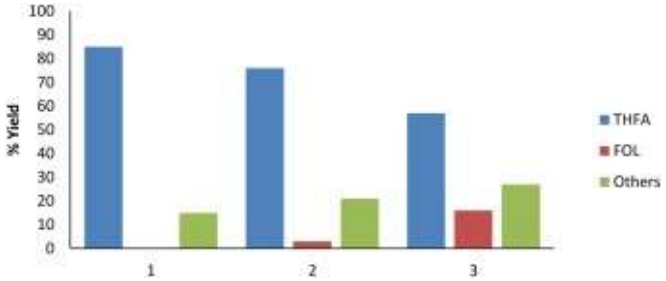

Fig. 11. Catalytic reuses of catalyst NiCu-DH.

After three reuses the conversion was total but the yield to THFA moderately decreased at expenses of the formation of FOL and other reaction byproducts. In order to explain this result, the reused catalyst was characterized by XRD and compared with the corresponding pattern of the fresh catalyst (Fig. 12).

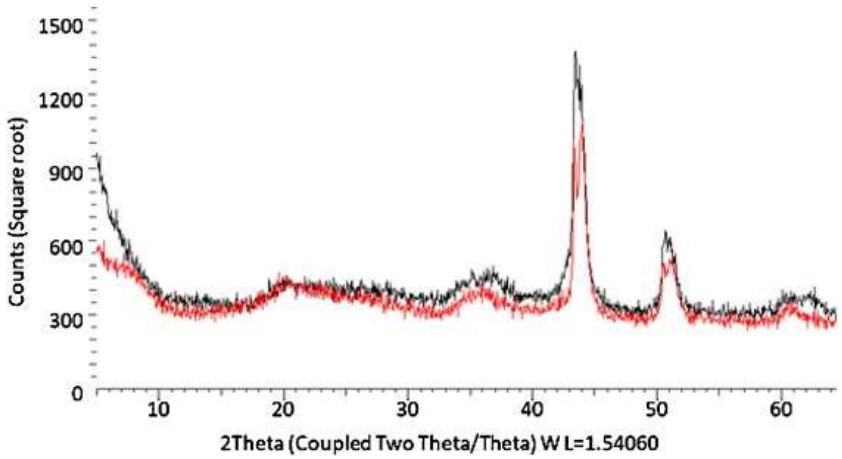

Fig. 12. XRD of the catalyst NiCu-DH before (black line) and after reaction (red line). (For interpretation of the references to colour in this figure legend, the reader is referred to the web version of this article).

XRD pattern of the reused catalyst showed the presence of the same crystalline phases (Cu and NiCu alloy) and in similar percentages than that taken for the fresh catalyst. However, an increase in the crystallinity of the Cu phase (114.4 nm of crystallite size in front of 31.8 nm for fresh catalyst) was detected. Taking into account the higher activity observed for the NiCu alloy phase, a decoration of the NiCu alloy particles by these bigger Cu particles can explain the decrease of the yield to THFA observed.

Conclusions

Catalytic precursors of bimetallic catalysts did not show the formation of solid solution due to the different structures of CuO and NiO. For the bimetallic catalysts with higher Cu content, a Cu2O phase was detected by XRD in low amounts in addition to NiO, CuO and hectorite phases. This was related to an increase of the well-known non-stoichiometric character of the nickel oxide, which could result in the oxidation of some Ni(II) atoms to Ni(III), allowing then the reduction of some Cu (II) atoms to Cu (I), as demonstrated by XPS. After reduction, XRD patterns of the NiCu bimetallic catalysts exhibited the presence in different amounts of NiCu alloy phase. The formation of this NiCu alloy together with the presence of higher amounts of Ni in the alloy has been related to a higher selectivity to THFA from the catalytic results. The highest selectivity to THFA (95 %) for a total conversion was achieved with the Ni-Cu catalyst prepared with Ni:Cu molar ratio 1:1 after 4 h of reaction. When using a biomass extract of furfural obtained from almond shells instead of commercial furfural, this catalyst resulted in a yield to THFA of 90 %, in the toluene phase, and 80 % in the aqueous neutralized phase. The increase in the crystallite size of the Cu after three reuses affected the activity of the NiCu alloy particles leading to a decrease in the yield to THFA.

CRediT authorship contribution statement

Vladimir Sánchez: Investigation, Visualization, Writing - original draft. Pilar Salagre: Conceptualization, Validation, Writing - original draft. María Dolores González: Conceptualization, Resources, Supervision. Jordi Llorca: Investigation, Validation. Yolanda Cesteros: Conceptualization, Resources, Supervision, Writing - original draft, Writing - review & editing.

Declaration of Competing Interest

The authors declare that they have no known competing financial interests or personal relationships that could have appeared to influence the work reported in this paper.

Acknowledgments

Authors acknowledge the finantial support of the Ministerio de Economía y Competitividad of Spain and Feder Funds (CTQ2015-70982-C3-3-R), and the recognition from the Generalitat de Catalunya

(2017 SGR 798). JL is a Serra Húnter Fellow and is grateful to ICREA Academia program and GC 2017 SGR 128.

References

[1] C.M. Cai, T. Zhang, R. Kumar, C.E. Wyman. Integrated furfural production as a renewable fuel and chemical platform from lignocellulosic biomass. J. Chem. Technol. Biotechnol., 89 (2014), pp. 2-10, 10.1002/jctb.4168

[2] Y. Nakagawa, M. Tamura, K. Tomishige. Catalytic conversions of furfural to Pentanediols. Catal. Surv. Asia, 19 (2015), pp. 249-256, 10.1007/s10563-015-9194-2

[3] C. Pischetola, L. Collado, M.A. Keane, F. Cárdenas-Lizana. Gas phase hydrogenation of furaldehydes via coupling with alcohol dehydrogenation over Ceria supported Au-Cu. Molecules, 23 (2018), p. 2905, 10.3390/molecules23112905

[4] Y. Nakagawa, K. Tomishige. Total hydrogenation of furan derivatives over silica-supported Ni–Pd alloy catalyst. Catal. Commun., 12 (2010), pp. 154-156, 10.1016/j.catcom.2010.09.003

[5] B.M. Matsagar, C. Hsu, S.S. Chen, T. Ahamad, S.M. Alshehri, D.C.W. Tsang, K.C.-W. Wu. Selective hydrogenation of furfural to tetrahydrofurfuryl alcohol over a Rh-loaded carbon catalyst in aqueous solution under mild conditions. Sustain. Energy Fuels, 4 (2020), pp. 293-301, 10.1039/C9SE00681H

[6] Y. Nakagawa, M. Tamura, K. Tomishige. Catalytic reduction of biomass-derived furanic compounds with hydrogen. ACS Catal., 3 (2013), pp. 2655-2668, 10.1021/cs400616p

[7] J. Wu, G. Gao, J. Li, P. Sun, X. Long, F. Li. Efficient and versatile CuNi alloy nanocatalysts for the highly selective hydrogenation of furfural. App. Catal. B: Environ., 203 (2017), pp. 227-236, 10.1016/j.apcatb.2016.10.038

[8] L. Liu, H. Lou, M. Chen. Selective hydrogenation of furfural to tetrahydrofurfuryl alcohol over Ni/CNTs and bimetallic Cu-Ni/CNTs catalysts. Int. J. Hydrog. Energy, 41 (2016), pp. 14721-14731, 10.1016/j.ijhydene.2016.05.188

[9] Y. Su, C. Chen, X. Zhu, Y. Zhang, W. Gong, H. Zhang, H. Zhao, G. Wang. Carbon-embedded Ni nanocatalysts derived from MOFs by a sacrificial template method for efficient hydrogenation of furfural to tetrahydrofurfuryl alcohol. Dalton Trans., 46 (2017), pp. 6358-6365, 10.1039/C7DT00628D

[10] S. Sang, Y. Wang, W. Zhu, G. Xiao. Selective hydrogenation of furfuryl alcohol to tetrahydrofurfuryl alcohol over Ni/γ-Al2O3 catalysts. Res. Chem. Intermed., 43 (2016), pp. 1179-1195, 10.1007/s11164-016-2691-8

[11] Y. Nakagawa, H. Nakazawa, H. Watanabe, K. Tomishige. Total hydrogenation of furfural over a silica-supported nickel catalyst prepared by the reduction of a nickel nitrate precursor. ChemCatChem, 4 (2012), pp. 1791-1797, 10.1002/cctc.201200218

[12] N. Hu, C. Yang, L. He, Q. Guan, R. Miao. Ni–Cu/Al2O3 catalysts for the selective hydrogenation of acetylene: a study on catalytic performance and reaction mechanism. New J. Chem., 43 (2019), pp. 18120-18125, 10.1039/C9NJ03956B

[13] K. Yan, Y. Liu, Y. Lu, L. Sun. Catalytic application of layered double hydroxide-derived catalysts for the conversion of biomass-derived molecules. Catal. Sci. Technol., 7 (2017), pp. 1622-1645, 10.1039/C7CY00274B

[14] J. Parikh, S. Srivastava, G.C. Jadeja. Selective hydrogenation of furfural to tetrahydrofurfuryl alcohol using supported Nickel-Cobalt Catalyst. Ind. Eng. Chem. Res., 58 (2019), pp. 16138-16152, 10.1021/acs.iecr.9b01443

[15] H. Wang, X. Li, X. Lan, T. Wang. Supported ultrafine NiCo bimetallic alloy nanoparticles derived from bimetal–organic frameworks: a highly active catalyst for furfuryl alcohol hydrogenation. ACS Catal., 8 (2018), pp. 2121-2128, 10.1021/acscatal.7b03795

[16] L. Ruan, H. Zhang, M. Zhou, L. Zhu, A. Pei, J. Wang, K. Yang, C. Zhang, S. Xiao, B.H. Chen. A highly selective and efficient Pd/Ni/Ni(OH)2/C catalyst for furfural hydrogenation at low temperatures. Mol. Catal., 480 (2020), Article 110639, 10.1016/j.mcat.2019.110639

[17] Y. Nakagawa, K. Takada, M. Tamura, K. Tomishige. Total hydrogenation of furfural and 5-hydroxymethylfurfural over supported Pd–Ir alloy catalyst. ACS Catal., 4 (2014), pp. 2718-2726, 10.1021/cs500620b

[18] K.A. Carrado. Synthetic organo- and polymer–clays: preparation, characterization, and materials applications. Appl. Clay Sci., 17 (2000), pp. 1-23, 10.1016/S0169-1317(00)00005-3

[19] F.-A. Khan, A. Vallat, G. Suss-Fink Highly selective low-temperature hydrogenation of furfuryl alcohol to tetrahydrofurfuryl alcohol catalysed by hectorite-supported ruthenium nanoparticles. Catal. Commun., 12 (2011), pp. 1428-1431, 10.1016/j.catcom.2011.05.024

[20] T. Iwasaki, M. Reinikainen, Y. Onodera, H. Hayashi, T. Ebina, T. Nagase, K. Torii, K. Kataja, A. Chatterjee. Use of silicate crystallite mesoporous material as catalyst support for Fischer–Tropsch reaction. Appl. Surf. Sci., 130–132 (1998), pp. 845-850, 10.1016/S0169-4332(98)00164-0

[21] K.A. Carrado, X. Langqiu. Materials with controlled mesoporosity derived from synthetic polyvinylpyrrolidone–clay composites. Microporous Mesoporous Mater., 27 (1999), pp. 87-94, 10.1016/S1387-1811(98)00275-3

[22] T. Sánchez, P. Salagre, Y. Cesteros, A. Bueno-López. Use of delaminated hectorites as supports of copper catalysts for the hydrogenolysis of glycerol to 1,2-propanediol. Chem. Eng. J., 179 (2012), pp. 302-311, 10.1016/j.cej.2011.11.011

[23] T. Sánchez, P. Salagre, Y. Cesteros. Ultrasounds and microwave-assisted synthesis of mesoporous hectorites. Microporous Mesoporous Mater., 171 (2013), pp. 24-34, 10.1016/j.micromeso.2013.01.001

[24] R.J. Hill, C.J. Howard. Quantitative phase analysis from neutron powder diffraction data using the Rietveld method. J. Appl. Cryst., 20 (1987), pp. 467-474, 10.1107/S0021889887086199

[25] D. Balzar. Voigt-function model in diffraction line-broadening analysis. R.L. Snyder, J. Fiala, H.J. Bunge (Eds.), Defect and Microstructure Analysis by Diffraction (International Union of Crystallography Monographs on Crystal), Oxford University Press, Oxford (1999), pp. 94-124

[26] H.M. Rietveld. A profile refinement method for nuclear and magnetic structures. J. Appl. Crystallogr., 2 (1969), pp. 65-71, 10.1107/S0021889869006558

[27] Bruker AXS GmbH. Software TOPAS 6 (2017)

[28] A.A. Coelho. TOPAS and TOPAS-Academic: An optimization program integrating computer algebra and crystallographic objects written in C++. J. Appl. Cryst., 51 (2018), pp. 210-218, 10.1107/S1600576718000183

[29] R.W. Cheary, A.A. Coelho, J.P. Cline. Fundamental parameters line profile fitting in laboratory diffractometers. J. Res. Inst. Stand. Technol., 109 (2004), pp. 1-25, 10.6028/jres.109.002

[30] A.R. Stokes, A.J.C. Wilson. A method of calculating the integral breadths of Debye-Scherrer lines. Math. Proc. Cambridge Philos. Soc., 38 (1942), pp. 313-322, 10.1017/S0305004100021988

[31] B. Małecka, A. Łącz, E. Drożdż, A. Małecki. Thermal decomposition of d-metal nitrates supported on alumina. J. Therm. Anal. Calorim., 119 (2015), pp. 1053-1061, 10.1007/s10973-014-4262-9

[32] A. Jha, D.W. Jeong, J.O. Shim, W.J. Jang, Y. Lim Lee, C.V. Rode, H.S. Roh. Hydrogen production by the water-gas shift reaction using CuNi/Fe2O3 catalyst. Catal. Sci. Technol., 5 (2015), pp. 2752-2760, 10.1039/c5cy00173k

[33] N. Gutta, V.K. Velisoju, A. Chatla, V. Boosa, J. Tardio, J. Patel, V. Akula. Promotional effect of Cu and influence of surface Ni−Cu alloy for enhanced H2 yields from CH4 decomposition over Cu-modified Ni supported on MCM-41 catalyst. Energy Fuels, 32 (2018), pp. 4008-4015, 10.1021/acs.energyfuels.7b03363

[34] A. Carrero, J.A. Calles, A.J. Vizcaíno. Effect of Mg and Ca addition on coke deposition over Cu–Ni/SiO2 catalysts for ethanol steam reforming. Chem. Eng. J., 163 (2010), pp. 395-402, 10.1016/j.cej.2010.07.029

[35] B.C. Miranda, R.J. Chiemntão, J. Sznayi, A.H. Braga, J.B.O. Santos, F. Gispert-Guirado, J. Llorca, F. Medina. Influence of copper on nickel-based catalysts in the conversion of glycerol. Appl. Catal. B: Environ., 166-167 (2015), pp. 166-180, 10.1016/j.apcatb.2014.11.019

[36] A. Kitla, O.V. Safonova, K. Föttinger. Infrared studies on bimetallic copper/nickel catalysts supported on zirconia and ceria/zirconia. Catal. Lett., 143 (2013), pp. 517-530, 10.1007/s10562-013-1001-y

[37] Y. Chen, Y. Yang, S. Tian, Z. Ye, Q. Tang, L. Ye, G. Li. Highly effective synthesis of dimethyl carbonate over CuNi alloy nanoparticles @Porous organic polymers composite. Appl. Catal. A Gen., 587 (2019), Article 117275, 10.1016/j.apcata.2019.117275